Report

Current Biology

Increased flexibility of CA3 memory representations following environmental enrichment

Highlights

- Environmental enrichment improves discrimination of similar associative memories
- EE-dependent memory improvements are related to increased adult neurogenesis
- EE results in sparser hippocampal activity
- EE increases spatial tuning, firing, and remapping of CA3 place cells

Authors

Silvia Ventura, Stephen Duncan, James A. Ainge

Correspondence

jaa7@st-andrews.ac.uk

In brief

Ventura et al. demonstrate that enrichment-dependent increases in adult hippocampal neurogenesis are associated with improved pattern separation in episodic-like memory in rats. Enrichment also results in sparser hippocampal neuronal activity as well as finer spatial tuning and increased remapping in CA3 place cells.

Ventura et al., 2024, Current Biology *34*, 1–9

https://doi.org/10.1016/j.cub.2024.03.054

CellPress

Please cite this article in press as: Ventura et al., Increased flexibility of CA3 memory representations following environmental enrichment, Current Biology (2024), https://doi.org/10.1016/j.cub.2024.03.054

Current Biology

CellPress
OPEN ACCESS

Report

Increased flexibility of CA3 memory representations following environmental enrichment

Silvia Ventura,[1] Stephen Duncan,[1,2] and James A. Ainge[1,3,*]
[1]School of Psychology & Neuroscience, University of St. Andrews, St. Mary's Quad, South Street, St. Andrews, Fife, Scotland KY16 9JP, UK
[2]School of Psychological & Brain Sciences, Indiana University, 1101 E 10th Street, Bloomington, IN 47405, USA
[3]Lead contact
*Correspondence: jaa7@st-andrews.ac.uk
https://doi.org/10.1016/j.cub.2024.03.054

SUMMARY

Environmental enrichment (EE) improves memory, particularly the ability to discriminate similar past experiences.[1–6] The hippocampus supports this ability via pattern separation, the encoding of similar events using dissimilar memory representations.[7] This is carried out in the dentate gyrus (DG) and CA3 subfields.[8–12] Upregulation of adult neurogenesis in the DG improves memory through enhanced pattern separation.[1–6,11,13–16] Adult-born granule cells (abGCs) in DG are suggested to contribute to pattern separation by driving inhibition in regions such as CA3,[13–18] leading to sparser, nonoverlapping representations of similar events (although a role for abGCs in driving excitation in the hippocampus has also been reported[16]). Place cells in the hippocampus contribute to pattern separation by remapping to spatial and contextual alterations to the environment.[19–27] How spatial responses in CA3 are affected by EE and input from increased numbers of abGCs in DG is, however, unknown. Here, we investigate the neural mechanisms facilitating improved memory following EE using associative recognition memory tasks that model the automatic and integrative nature of episodic memory. We find that EE-dependent improvements in difficult discriminations are related to increased neurogenesis and sparser memory representations across the hippocampus. Additionally, we report for the first time that EE changes how CA3 place cells discriminate similar contexts. CA3 place cells of enriched rats show greater spatial tuning, increased firing rates, and enhanced remapping to contextual changes. These findings point to more precise and flexible CA3 memory representations in enriched rats, which provides a putative mechanism for EE-dependent improvements in fine memory discrimination.

RESULTS AND DISCUSSION

Improved discrimination of similar associative memories and increased adult hippocampal neurogenesis following environmental enrichment (EE)

Adult hippocampal neurogenesis has been consistently implicated in pattern separation.[11,13,28,29] However, many pattern separation tests fail to model key features of episodic memory such as automatic encoding and integration of episodic memory features.[30,31] To address this, we examined discrimination of similar contextual memories during associative recognition memory tasks which test memory for automatically encoded, integrated features of events. These tasks require context and location-specific memories both of which have been shown to require the hippocampus.[32–34] Enriched and standard-housed rats (Figure S1A) were tested using the object-context (OC) and object-place-context (OPC) tasks, which test memory for associations of objects with places and/or contexts and depend on the hippocampus,[35] but also see Langston and Wood[36] and Norman and Eacott.[37] These tasks were chosen for two reasons. Firstly, the context changes in these tasks are similar to those used in place cell studies examining mechanisms for encoding similar events.[8,22] Secondly, these tasks are also dependent on the lateral entorhinal cortex (LEC),[38–41] which provides the strongest input to adult-born granule cells (abGCs) in their first few weeks.[42,43] To manipulate the overlap in contextual information, the animals were tested on two versions of the tasks (Figures 1A and 1B). In the similar condition, the contexts used were the square and circle versions of a "morph" box (Figure S1B). In the dissimilar condition, the contexts were distinct boxes with different walls and floors making them easier to discriminate.

Enriched rats (EE, n = 12) performed significantly better than standard-housed rats (ST, n = 12) in the similar ($F_{(1,21)} = 6.092$, $p = 0.022$, $\eta_p^2 = 0.22$), but not in the dissimilar ($F_{(1,21)} = 0.002$, $p = 0.962$, $\eta_p^2 = 0.000$), OC task (Figure 1C), pointing to a selective enrichment-dependent improvement in fine associative memory discrimination. Critically, while both groups performed above chance level in the dissimilar OC task—showing successful discrimination of distinct contextual memories—only the enriched rats performed above chance level when more similar contexts were used. In the OPC task, only the enriched rats showed memory for the similar OPC memories. However, there was no significant difference in group performance in either similar or dissimilar OPC task (similar: $F_{(1,21)} = 0.762$, $p = 0.393$, $\eta_p^2 = 0.035$; dissimilar: $F_{(1,21)} = 0.958$, $p = 0.339$, $\eta_p^2 = 0.044$) (Figure 1D). While the trend of results across the two tasks is similar, the enhancement of difficult memory discriminations in

Please cite this article in press as: Ventura et al., Increased flexibility of CA3 memory representations following environmental enrichment, Current Biology (2024), https://doi.org/10.1016/j.cub.2024.03.054

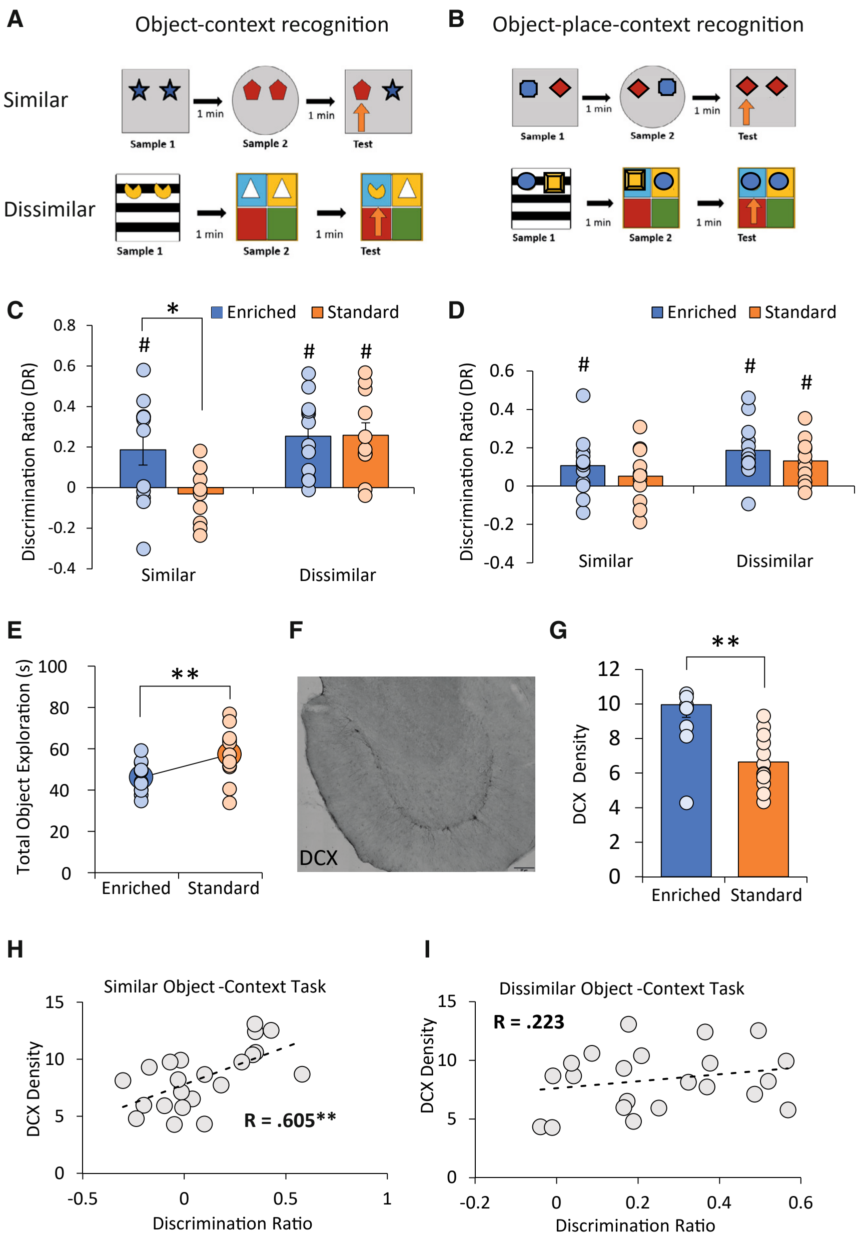

Figure 1. Improved discrimination of similar associative memories and increased adult hippocampal neurogenesis following EE

(A and B) Schematic of the OC (A) and OPC (B) recognition memory tasks (top, similar; bottom, dissimilar). Orange arrow indicates a novel configuration.

(C and D) Average discrimination ratios (DRs) for the similar and dissimilar OC (C) and OPC (D) tasks.

(E) Total object exploration during encoding of the OC and OPC tasks.

(F) Doublecortin (DCX) in the DG. Scale bars, 37 mm.

(G) Average density of DCX + cells in DG.

(H and I) Scatterplots of DCX+ density plotted against DRs for the similar OC (H) and dissimilar OC (I) tasks. $*p < 0.05$, $**p < 0.01$, $***p < 0.001$. Dots indicate single animals. Error bars: SEM. # greater than 0 ($p < 0.05$).

See also Figures S1 and S2.

the enriched rats was only seen in the OC. This is likely due to overall lower levels of performance in the OPC task. Interestingly, the enriched rats spent less time exploring the objects during encoding (Figure 1E). To check for differences in movement behavior we quantified running speed, thigmotaxis (% time within 10 cm of the wall), and rearing. There were no significant group differences in any of these measures (Figures S2A–S2C). Together, these findings suggest that environmental enrichment (EE) leads to improved memory discrimination of similar contextual features of episodic-like memories and more efficient encoding of novel associations in episodic memory.

Next, we examined adult hippocampal neurogenesis in the dorsal hippocampus (Figure 1F) by measuring the density of doublecortin (DCX+) cells. Enriched rats had increased DCX+ cell density in DG compared with standard-housed rats ($F_{(1,21)} = 15.10$, $p < 0.001$, $\eta_p^2 = 0.42$) (Figure 1G). Additionally, there was a significant positive correlation between adult hippocampal neurogenesis and performance in the similar, but not in the dissimilar, OC task (similar: $r_{(22)} = 0.605$, $p = 0.003$; dissimilar: $r_{(22)} = 0.223$, $p = 0.852$) (Figures 1H and 1I). There was, however, no correlation between performance in the OPC tasks and adult hippocampal neurogenesis, again likely due to the generally lower levels of performance in the OPC task (Figures S1C and S1D). These findings show that EE leads to greater levels of adult hippocampal neurogenesis, and improved discrimination of similar context-dependent associative memories.

Increased sparsity of activity in the hippocampus of enriched rats

Previous studies point to EE changing how hippocampal ensembles encode different memories. EE has been shown to lead to sparser memory representations in CA1 place cells,[44] while other studies have suggested that abGCs might drive increased excitation in the hippocampus.[16] Consistent with the inhibitory hypothesis, immature abGCs, which are upregulated by EE,[45] drive inhibition across the hippocampus.[13–18] Increased hippocampal inhibition is thought to promote pattern separation of similar events and reduce interference.[29] Before going on to look at the specific effects of EE on the principle afferent connections of GCs (including abGCs) in CA3, we first sought to examine how EE affects activity across the whole hippocampal network. We assessed whether EE resulted in increased hippocampal sparsity as rats explored novel and familiar OC associations using c-Fos as a marker for neural activity. Rats explored two objects within a context (square or circle) over 2 days. On day 3, rats either experienced the same objects within the same context (familiar condition) or another context (novel condition) (Figure 2A). This allowed us to assess

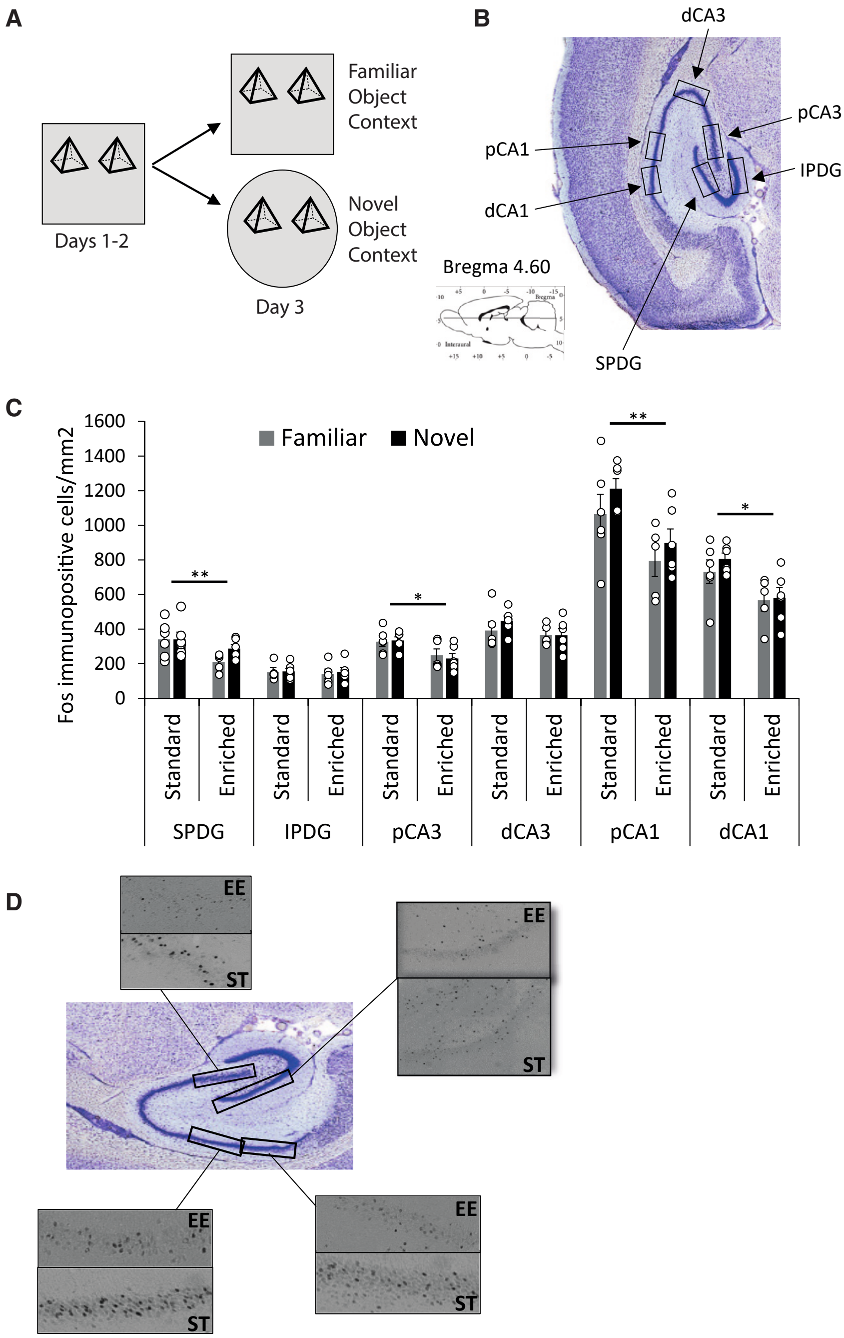

Figure 2. Increased sparsity of activity in the hippocampus of enriched rats

(A) Schematic of the novel and familiar conditions.

(B) Horizontal section stained with NeuN. Black boxes indicate regions of interest (ROIs). SPDG, suprapyramidal dentate gyrus; IPDG, infrapyramidal dentate gyrus; pCA3, proximal CA3; dCA3, distal CA3; pCA1, proximal CA1; dCA1, distal CA1.

(C) Average *c-fos* cell densities across the hippocampus.

(D) Representative images of *c-fos* expression from the SPDG, pCA3, pCA1, and dCA1 of the enriched and standard-housed rats. *$p < 0.05$, **$p < 0.01$. Error bars: SEM.

the effects of EE on hippocampal activity in response to novel and familiar OC configurations.

EE led to reduced activation across the hippocampus in response to both novel and familiar OC configurations ($F_{(1,19)} = 8.194$, $p = 0.010$, $\eta_p^2 = 0.775$) (Figures 2B and 2C). However, there was no significant interaction of enrichment group and novelty condition ($F_{(1,19)} = 0.003$, $p = 0.959$, $\eta_p^2 = 0.050$) or three-way interaction of group, condition, and hippocampal subregion ($F_{(5,15)} = 0.776$, $p = 0.582$, $\eta_p^2 = 0.207$), which shows that enrichment was associated with sparser activity in response to both novel and familiar OC configurations. There was, however, a significant hippocampal subregion and enrichment group interaction ($F_{(5,15)} = 3.220$, $p = 0.036$, $\eta_p^2 = 0.739$). Post hoc analyses revealed significantly reduced activation in enriched rats relative to standard-housed rats in suprapyramidal dentate gyrus (SPDG) ($p = 0.016$), proximal CA3 ($p = 0.005$), and proximal and distal CA1 ($p = 0.004$ and $p = 0.003$, respectively) (Figures 2C and 2D). Together, these findings show that EE leads to sparser hippocampal memory representations of both novel and familiar OC associations.

Increased spatial tuning and firing rates of CA3 place cells of enriched rats

To investigate the effect of EE on place cell activity, we implanted tetrodes in CA3 of enriched ($n = 5$) and standard-housed rats ($n = 5$) (Figure 3A). We focused on CA3 as this subregion receives direct input from granule cells in DG, and so this is where we would expect changes induced by increased neurogenesis to be seen.[14,42] Surprisingly, the effects of EE and increased numbers of abGCs on CA3 place cells have not yet been investigated. Place cells were recorded as rats explored the distinct versions of a morph box that could be shaped as a square, a circle, or as four intermediate shapes.[46–48] Each session began with an exploration of the square or circle, followed by an exploration of the intermediate shapes, the opposite shape (circle or square), and a repetition of the first shape (Figure S3B). Analysis of CA3 place fields from the square box (10 rats; 5 enriched, 5 standard, Table S1) showed that enriched rats had smaller place fields (Figure 3C) ($H_{(1)} = 6.948$, $p = 0.008$) that carried greater spatial information (Figure 3D) ($H_{(1)} = 19.115$, $p < 0.001$) compared with standard-housed rats. EE also reduced sparseness of firing (Figure 3E) ($H_{(1)} = 19.546$, $p < 0.001$), enhanced spatial selectivity (Figure 3F) ($H_{(1)}$ 16.821, $p < 0.001$), and increased firing rates (average in-field rate, $H_{(1)} = 13.700$, $p < 0.001$; peak rate, $H_{(1)}$ =12.381, $p < 0.001$) (Figures 3G and 3H). EE had no significant effect on interspike interval, % bursting, or theta modulation (Figures 3I–3L). Together, these findings show

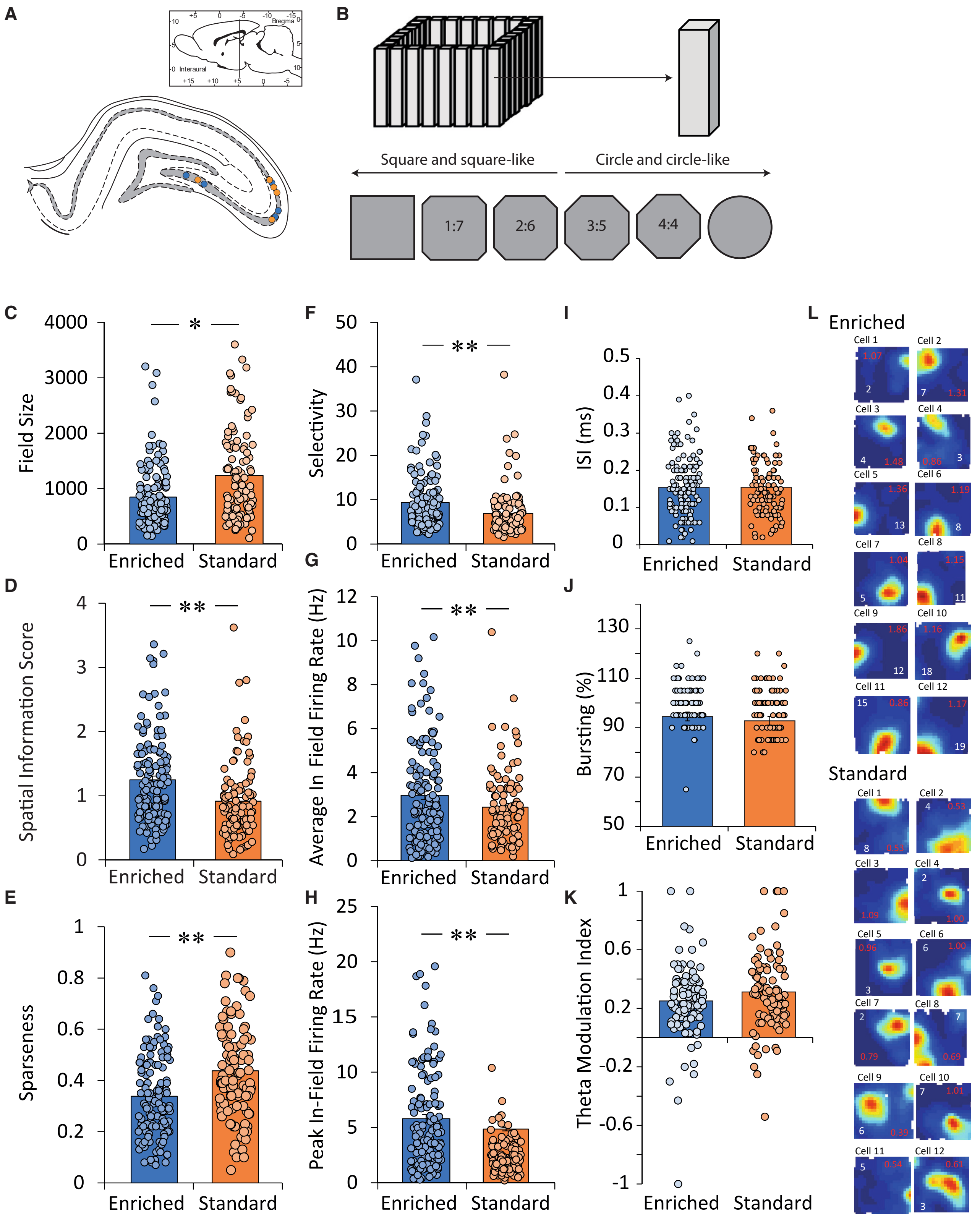

Figure 3. Increased spatial tuning and firing rates of CA3 place cells of enriched rats

(A) Tetrode locations from the enriched (blue) and standard-housed (orange) rats.

(B) Morph box shaped as a square (top) and the morph environments (bottom).

(legend continued on next page)

the increased spatial tuning of CA3 place cells in the enriched rats accompanied by an increase in gain, signaled by the upregulation of firing rates.

Enhanced place cell remapping and increased subset switching in CA3 place cells of enriched rats

Next, we assessed whether EE modulates CA3 place cell remapping in the morph box. We first analyzed all cells that had a field in each of the 7 configurations of the morph box within a recording session (full sequence) (Figures 4A, 4B, and S3B; Table S1). A significant trial × group interaction showed that CA3 place cells from the enriched rats have different patterns of rate remapping across shapes relative to those from standard-housed rats ($F_{(5,505)} = 2.295$, $p = 0.034$, $\eta_p^2 = 0.022$). Post hoc analyses showed that rate remapping was similar between groups when shapes were similar but that place cells from enriched rats showed significantly more rate remapping as the shapes became more different (Figures 4B and 4D). Given that many place cells were recorded from sessions that did not include all shapes of the morph sequence (partial sequences) (Figure S3B), we ran a generalized linear mixed model (GLMM), including both full and partial sequences to see if increased rate remapping was present even when shorter sequences were included. CA3 place cells from the enriched rats showed increased rate remapping across the sequence ($F_{(1,1203)} = 7.653$, $p = 0.006$) (Figures 4C and 4D). Again, EE led to increased rate remapping across the square and the circle shapes, as well as across the square and the most circle-like shapes. Interestingly, in this sample, CA3 place cells in the enriched rats also showed increased rate remapping in response to the delayed exploration of the initial shape. Together, these findings point to EE resulting in increased flexibility in the CA3 spatial map.

To examine whether changes in shape induced a change in the map, we next examined global remapping. We started by examining the same pool of cells used for the rate remapping (full and partial sequences) (Figures 4E and S3A). Spatial correlations between rate maps within the session remained high (Figure 2E) and there was no difference in spatial correlations across groups ($F_{(1,245.912)} = 0.699$, $p = 0.404$). This shows that CA3 place cells encode fine contextual changes using rate rather than global remapping.[46–48] We next assessed whether EE influenced global remapping across the morph sequence in all recorded place cells (Figure 4F; Table S1). Again, there was no difference in spatial correlation values for the place cells across groups (Figure 4F) ($F_{(1,346.18)} = 1.302$, $p = 0.255$). Together, these findings suggest that EE does not alter the global remapping of CA3 place fields.

Place cells might also discriminate between distinct environments by switching on and off as the environment changes (subset switching[19,49]). EE increases CA1 subset switching as rats explore distinct environments.[44] We compared the percentage of place cells active in at least one, but not all, environments across groups. A greater percentage of place cells exhibited subset switching in the enriched rats (EE: 44/196 place cells, 22.4%; ST: 15/160 place cells; 9.4%) ($\chi^2_{(1)} = 10.890$, $p < 0.001$) (Figure 4G) even when conducting the analysis on a per animal basis ($t_{(8)} = 2.541$, $p = 0.035$, $d' = 8.360$) (Figure S4A). These findings point to more specific encoding of environments following EE.

Finally, as we recorded place cells along the CA3 transverse axis (Figure 4H), we assessed whether there was a relationship between remapping scores and tetrode location. There was a significant negative correlation between tetrode location and rate difference ($r_{(7)} = -0.811$, $p = 0.027$) (Figure 4I; Table S2). There were, however, no correlations between tetrode location and place cell properties (Table S3), spatial correlation (Figure S4B), or subset switching (Figure S4C). This finding points to greater rate remapping in place cells recorded from the most proximal CA3, compared with distal CA3.

Here, we investigated putative neural mechanisms supporting enrichment-dependent memory improvements using behavioral tasks that model episodic memory. We found that EE-dependent improvements in fine memory discrimination are related to increased adult hippocampal neurogenesis and enhanced sparsity of neuronal activity across the hippocampus. We also found that EE changes the way CA3 encodes changes in context. EE leads to increased spatial tuning of CA3 place cells, as CA3 place cells in enriched rats carry greater spatial information, have higher firing rates, and show increased remapping in response to small contextual changes to the environment. These findings are consistent with research showing that adult hippocampal neurogenesis is fundamental for pattern separation.[11] The current studies extend this research in two important ways. Firstly, by modeling key features of episodic memory, we extend previous findings to the most clinically relevant form of memory. Secondly, we demonstrate enrichment-dependent changes in CA3 place cells, the region that receives input directly from abGCs,[14,42] for the first time.

Interestingly, EE-dependent increased sparsity was particularly evident in the SPDG, compared with the infrapyramidal dentate gyrus (IPDG). Given that the SPDG receives most input from LEC,[50] these findings support research suggesting that immature abGCs drive inhibition in response to LEC input.[16] This increased inhibition in the SPDG, rather than in the IPDG, is related to improved pattern separation.[51] Additionally, the finding that EE results in reduced activity in proximal, rather than in distal, CA3 points to a special role for proximal CA3 in pattern separation. This is consistent with previous research[9,10,52] and with our finding of greater rate remapping in cells recorded from proximal, rather than distal, CA3.

The increased spatial tuning of CA3 place cells in enriched rats suggests that EE leads to more precise spatial information encoding in CA3. Combined with reports of enrichment-dependent increases of spatial tuning and spatial information in DG granule cells in novel environments,[53] these findings show that EE has

(C–H) Bar graphs comparing field size (C), spatial information score (D), sparseness (E), selectivity (F), average firing rate (G), and peak firing rate (H).
(I–K) Interspike interval (ISI) (I), % bursting (J), and theta modulation index (K) across the enriched and the standard-housed rats. *$p < 0.01$, **$p < 0.001$. Dots indicate values for single place fields. Error bars: SEM.
(L) Rate maps from representative cells from enriched (top) and standard (bottom) rats. Warm colors, high firing rates; cool colors, low firing rates. Peak firing rates are shown in white; spatial information scores are in red.
See also Tables S1 and S3.

Please cite this article in press as: Ventura et al., Increased flexibility of CA3 memory representations following environmental enrichment, Current Biology (2024), https://doi.org/10.1016/j.cub.2024.03.054

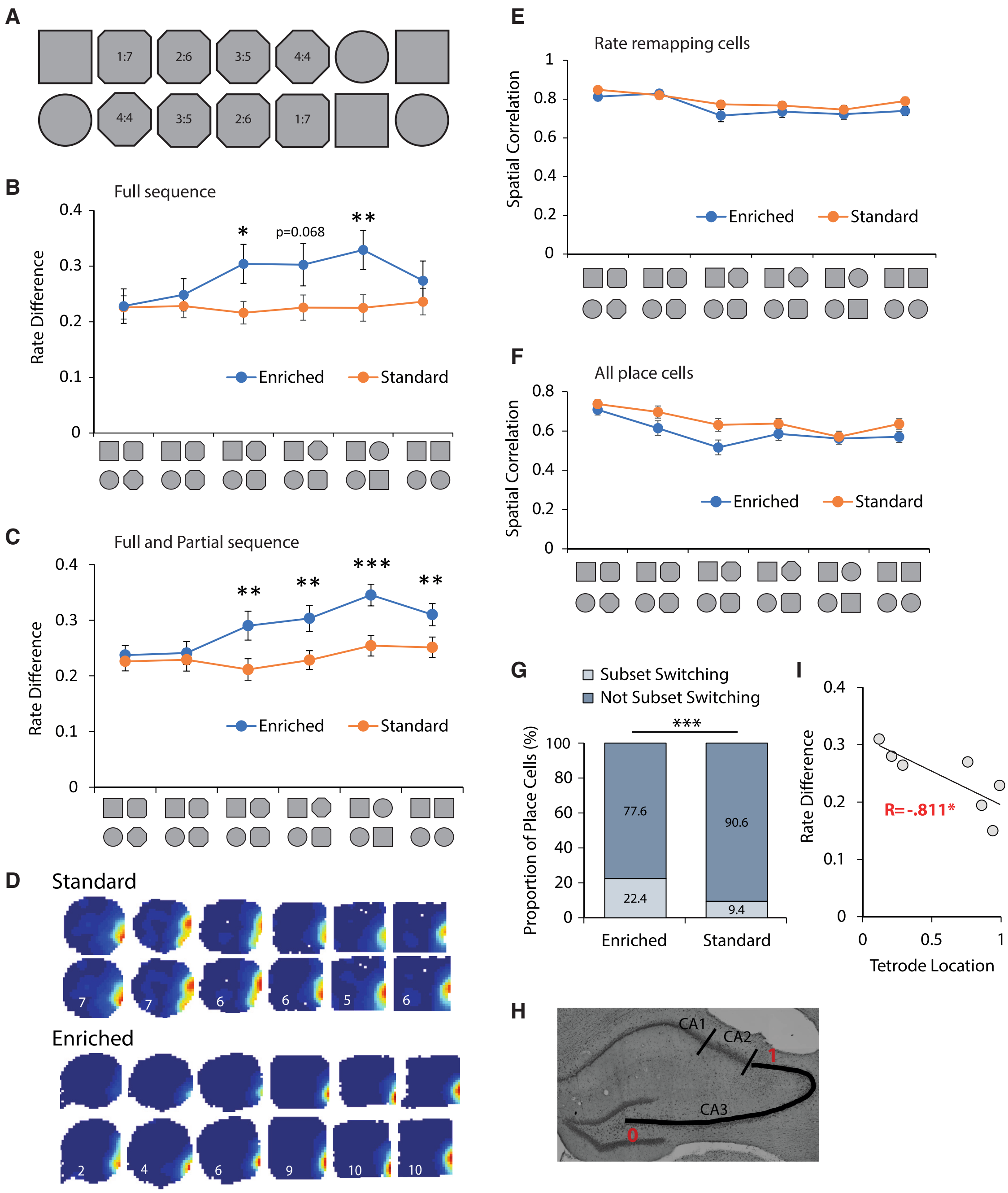

Figure 4. Enhanced place cell remapping and increased subset switching in CA3 place cells of enriched rats

(A) Schematic of the full sequence.

(B and C) Average rate remapping across the first shape in the sequence and each subsequent shape for cells with place fields in the full sequence of environments (B) or fields in either the full or partial sequence of environments (C).

(D) Example place cells recorded across the full sequence from the standard (top) and enriched (bottom) rats. For each cell, maps are shown scaled to the maximum firing rates across all environments (top) and to the maximum firing rate within a session (bottom).

(E and F) Average spatial correlation scores across the first shape in the sequence and each subsequent shape for the sample of cells that showed rate remapping (E) and for the full sample of place cells (F).

(G) Proportion of place cells showing subset switching across the recording sequence.

(H) Tetrode location across the proximodistal axis of CA3. 0, most proximal; 1, most distal.

(I) Tetrode location plotted against the rate remapping values across the full sequence for enriched and standard-housed rats. *$p < 0.05$, **$p < 0.01$, ***$p < 0.001$. Error bars: SEM.

See also Figures S3 and S4 and Tables S2 and S3.

clear effects on spatial tuning of place cells in the DG/CA3 network. This stands in contrast to findings from CA1.[44]

EE also resulted in increased firing rates in CA3 place cells which contrasts with studies showing that increased neurogenesis is typically associated with decreased activity in the DG and CA3[13–18] (but see also Luna et al.[16]). This discrepancy, however, comes from the way activity is measured. Studies examining how EE and adult hippocampal neurogenesis modulate hippocampal activity examined differences in the percentage of active neurons.[44] The findings of this study suggest that EE reduces the number of active cells while increasing the activity of those cells. This allows the hippocampus to reduce interference by encoding spatial information using a small neuronal population with high spatial information.[53]

We also report an enrichment-dependent increase in CA3 rate remapping. Interestingly, our standard-housed rats did not show CA3 rate remapping as previously reported.[46–48] This can potentially be explained by slightly different protocols. Here, morph box shapes were made as similar as possible. Previous studies have used different floors and colors for each shape and extensive pretraining.[46–48] This makes the discrimination between shapes in our study harder, which might explain the lack of rate remapping in our standard-housed rats.

One caveat here is that we did not measure memory directly in the rats from which place cell recordings were taken; therefore, we cannot causally link the changes in place cell properties reported here with memory improvements. Future studies could aim to record from place cells as rats carry out fine memory discriminations. One final issue that will need to be addressed in the future is that, while these results show a significant positive correlation between abGCs and memory, we cannot rule out the possibility that other EE-induced changes may support improved memory.

In summary, we report for the first time that EE changes the way the CA3 place cells encode spatial environments by increasing their spatial tuning and chances of remapping. Together, these findings point to more precise, and more flexible, memory representations in the CA3 of enriched rats. This increase in spatial tuning and in the ability to respond to alterations to familiar environments might provide a novel neuronal mechanism for enrichment-dependent improvements in fine memory discrimination.

STAR★METHODS

Detailed methods are provided in the online version of this paper and include the following:

- KEY RESOURCES TABLE
- RESOURCE AVAILABILITY
  - Lead contact
  - Materials availability
  - Data and code availability
- EXPERIMENTAL MODEL AND SUBJECT DETAILS
  - Animals
- METHOD DETAILS
  - Housing conditions
  - Behavioural experiment & Fos experiment
  - Recording experiment
- QUANTIFICATION AND STATISTICAL ANALYSIS

SUPPLEMENTAL INFORMATION

Supplemental information can be found online at https://doi.org/10.1016/j.cub.2024.03.054.

ACKNOWLEDGMENTS

We thank the members of the St Mary's Animal Unit (SMAU) for their support and advice on the environmental enrichment used in these experiments. This work was supported by a grant from the BBSRC (BB/X007197/1).

AUTHOR CONTRIBUTIONS

Conceptualization and methodology, S.V. and J.A.A. Investigation, S.V. Formal analysis, S.V., S.D., and J.A.A. Resources, J.A.A. Writing—original draft, S.V. Writing—review and editing, J.A.A. and S.V. Supervision, J.A.A. Funding acquisition, J.A.A.

DECLARATION OF INTERESTS

The authors declare no competing interests.

Received: November 17, 2023
Revised: February 16, 2024
Accepted: March 25, 2024
Published: April 17, 2024

REFERENCES

1. Bolz, L., Heigele, S., and Bischofberger, J. (2015). Running Improves Pattern Separation during Novel Object Recognition. Brain Plast. *1*, 129–141. https://doi.org/10.3233/BPL-150010.
2. Clemenson, G.D., Lee, S.W., Deng, W., Barrera, V.R., Iwamoto, K.S., Fanselow, M.S., and Gage, F.H. (2015). Enrichment rescues contextual discrimination deficit associated with immediate shock. Hippocampus *25*, 385–392. https://doi.org/10.1002/hipo.22380.
3. Frick, K.M., Stearns, N.A., Pan, J.Y., and Berger-Sweeney, J. (2003). Effects of environmental enrichment on spatial memory and neurochemistry in middle-aged mice. Learn. Mem. *10*, 187–198. https://doi.org/10.1101/lm.50703.
4. Meshi, D., Drew, M.R., Saxe, M., Ansorge, M.S., David, D., Santarelli, L., Malapani, C., Moore, H., and Hen, R. (2006). Hippocampal neurogenesis is not required for behavioral effects of environmental enrichment. Nat. Neurosci. *9*, 729–731. https://doi.org/10.1038/nn1696.
5. Mora-Gallegos, A., Rojas-Carvajal, M., Salas, S., Saborío-Arce, A., Fornaguera-Trías, J., and Brenes, J.C. (2015). Age-dependent effects of environmental enrichment on spatial memory and neurochemistry. Neurobiol. Learn. Mem. *118*, 96–104. https://doi.org/10.1016/j.nlm.2014.11.012.
6. Garthe, A., Roeder, I., and Kempermann, G. (2016). Mice in an enriched environment learn more flexibly because of adult hippocampal neurogenesis. Hippocampus *26*, 261–271. https://doi.org/10.1002/hipo.22520.
7. Rolls, E.T., and Kesner, R.P. (2006). A computational theory of hippocampal function, and empirical tests of the theory. Prog. Neurobiol. *79*, 1–48. https://doi.org/10.1016/j.pneurobio.2006.04.005.
8. Leutgeb, J.K., Leutgeb, S., Moser, M.B., and Moser, E.I. (2007). Pattern Separation in the Dentate Gyrus and CA3 of the Hippocampus. Science *315*, 961–966. https://doi.org/10.1126/science.1135801.
9. Lee, H., GoodSmith, D., and Knierim, J.J. (2020). Parallel processing streams in the hippocampus. Curr. Opin. Neurobiol. *64*, 127–134. https://doi.org/10.1016/j.conb.2020.03.004.
10. GoodSmith, D., Lee, H., Neunuebel, J.P., Song, H., and Knierim, J.J. (2019). Dentate Gyrus Mossy Cells Share a Role in Pattern Separation with Dentate Granule Cells and Proximal CA3 Pyramidal Cells. J. Neurosci. *39*, 9570–9584. https://doi.org/10.1523/JNEUROSCI.0940-19.2019.
11. Clelland, C.D., Choi, M., Romberg, C., Clemenson, G.D., Jr., Fragniere, A., Tyers, P., Jessberger, S., Saksida, L.M., Barker, R.A., Gage, F.H., and

Bussey, T.J. (2009). A functional role for adult hippocampal neurogenesis in spatial pattern separation. Science *325*, 210–213. https://doi.org/10.1126/science.1173215.

12. Bekinschtein, P., Kent, B.A., Oomen, C.A., Clemenson, G.D., Gage, F.H., Saksida, L.M., and Bussey, T.J. (2013). BDNF in the dentate gyrus is required for consolidation of "pattern-separated" memories. Cell Rep. *5*, 759–768. https://doi.org/10.1016/j.celrep.2013.09.027.

13. McAvoy, K., Besnard, A., and Sahay, A. (2015). Adult hippocampal neurogenesis and pattern separation in DG: a role for feedback inhibition in modulating sparseness to govern population-based coding. Front. Syst. Neurosci. *9*, 120. https://doi.org/10.3389/fnsys.2015.00120.

14. Restivo, L., Niibori, Y., Mercaldo, V., Josselyn, S.A., and Frankland, P.W. (2015). Development of Adult-Generated Cell Connectivity with Excitatory and Inhibitory Cell Populations in the Hippocampus. J. Neurosci. *35*, 10600–10612. https://doi.org/10.1523/JNEUROSCI.3238-14.2015.

15. Niibori, Y., Yu, T.S., Epp, J.R., Akers, K.G., Josselyn, S.A., and Frankland, P.W. (2012). Suppression of adult neurogenesis impairs population coding of similar contexts in hippocampal CA3 region. Nat. Commun. *3*, 1253. https://doi.org/10.1038/ncomms2261.

16. Luna, V.M., Anacker, C., Burghardt, N.S., Khandaker, H., Andreu, V., Millette, A., Leary, P., Ravenelle, R., Jimenez, J.C., Mastrodonato, A., et al. (2019). Adult-born hippocampal neurons bidirectionally modulate entorhinal inputs into the dentate gyrus. Science *364*, 578–583. https://doi.org/10.1126/science.aat8789.

17. Cahill, S.P., Martinovic, A., Cole, J.D., Seib, D.R., and Snyder, J.S. (2019). A combination of running and memantine increases neurogenesis and reduces activation of developmentally-born dentate granule neurons in rats. Behav. Brain Res. *372*, 112005. https://doi.org/10.1016/j.bbr.2019.112005.

18. McHugh, S.B., Lopes-Dos-Santos, V., Gava, G.P., Hartwich, K., Tam, S.K.E., Bannerman, D.M., and Dupret, D. (2022). Adult-born dentate granule cells promote hippocampal population sparsity. Nat. Neurosci. *25*, 1481–1491. https://doi.org/10.1038/s41593-022-01176-5.

19. Muller, R.U., and Kubie, J.L. (1987). The effects of changes in the environment on the spatial firing of hippocampal complex-spike cells. J. Neurosci. *7*, 1951–1968. https://doi.org/10.1523/JNEUROSCI.07-07-01951.1987.

20. O'Keefe, J., and Burgess, N. (1996). Geometric determinants of the place fields of hippocampal neurons. Nature *381*, 425–428. https://doi.org/10.1038/381425a0.

21. Kentros, C., Hargreaves, E., Hawkins, R.D., Kandel, E.R., Shapiro, M., and Muller, R.V. (1998). Abolition of long-term stability of new hippocampal place cell maps by NMDA receptor blockade. Science *280*, 2121–2126. https://doi.org/10.1126/science.280.5372.2121.

22. Wills, T.J., Lever, C., Cacucci, F., Burgess, N., and O'Keefe, J. (2005). Attractor dynamics in the hippocampal representation of the local environment. Science *308*, 873–876. https://doi.org/10.1126/science.1108905.

23. Leutgeb, S., Leutgeb, J.K., Barnes, C.A., Moser, E.I., McNaughton, B.L., and Moser, M.B. (2005). Independent codes for spatial and episodic memory in hippocampal neuronal ensembles. Science *309*, 619–623. https://doi.org/10.1126/science.1114037.

24. Wood, E.R., Dudchenko, P.A., Robitsek, R.J., and Eichenbaum, H. (2000). Hippocampal neurons encode information about different types of memory episodes occurring in the same location. Neuron *27*, 623–633. https://doi.org/10.1016/s0896-6273(00)00071-4.

25. Ainge, J.A., Tamosiunaite, M., Wörgötter, F., and Dudchenko, P.A. (2012). Hippocampal place cells encode intended destination, and not a discriminative stimulus, in a conditional T-maze task. Hippocampus *22*, 534–543. https://doi.org/10.1002/hipo.20919.

26. Vandrey, B., Duncan, S., and Ainge, J.A. (2021). Object and object-memory representations across the proximodistal axis of CA1. Hippocampus *31*, 881–896. https://doi.org/10.1002/hipo.23331.

27. Ainge, J.A., van der Meer, M.A., Langston, R.F., and Wood, E.R. (2007). Exploring the role of context-dependent hippocampal activity in spatial alternation behavior. Hippocampus *17*, 988–1002. https://doi.org/10.1002/hipo.20301.

28. Creer, D.J., Romberg, C., Saksida, L.M., van Praag, H., and Bussey, T.J. (2010). Running enhances spatial pattern separation in mice. Proc. Natl. Acad. Sci. USA *107*, 2367–2372. https://doi.org/10.1073/pnas.0911725107.

29. Miller, S.M., and Sahay, A. (2019). Functions of adult-born neurons in hippocampal memory interference and indexing. Nat. Neurosci. *22*, 1565–1575. https://doi.org/10.1038/s41593-019-0484-2.

30. Eacott, M.J., and Norman, G. (2004). Integrated memory for object, place, and context in rats: a possible model of episodic-like memory? J. Neurosci. *24*, 1948–1953. https://doi.org/10.1523/JNEUROSCI.2975-03.2004.

31. Clayton, N.S., and Dickinson, A. (1998). Episodic-like memory during cache recovery by scrub jays. Nature *395*, 272–274. https://doi.org/10.1038/26216.

32. Rudy, J.W. (2009). Context representations, context functions, and the parahippocampal-hippocampal system. Learn. Mem. *16*, 573–585. https://doi.org/10.1101/lm.1494409.

33. Maren, S. (2008). Pavlovian fear conditioning as a behavioral assay for hippocampus and amygdala function: cautions and caveats. Eur. J. Neurosci. *28*, 1661–1666. https://doi.org/10.1111/j.1460-9568.2008.06485.x.

34. Sill, O.C., and Smith, D.M. (2012). A comparison of the effects of temporary hippocampal lesions on single and dual context versions of the olfactory sequence memory task. Behav. Neurosci. *126*, 588–592. https://doi.org/10.1037/a0028824.

35. Mumby, D.G., Gaskin, S., Glenn, M.J., Schramek, T.E., and Lehmann, H. (2002). Hippocampal Damage and Exploratory Preferences in Rats: Memory for Objects, Places, and Contexts. Learn. Mem. *9*, 49–57. https://doi.org/10.1101/lm.41302.

36. Langston, R.F., and Wood, E.R. (2010). Associative recognition and the hippocampus: differential effects of hippocampal lesions on object-place, object-context and object-place-context memory. Hippocampus *20*, 1139–1153. https://doi.org/10.1002/hipo.20714.

37. Norman, G., and Eacott, M.J. (2005). Dissociable effects of lesions to the perirhinal cortex and the postrhinal cortex on memory for context and objects in rats. Behav. Neurosci. *119*, 557–566. https://doi.org/10.1037/0735-7044.119.2.557.

38. Wilson, D.I., Langston, R.F., Schlesiger, M.I., Wagner, M., Watanabe, S., and Ainge, J.A. (2013). Lateral entorhinal cortex is critical for novel object-context recognition. Hippocampus *23*, 352–366. https://doi.org/10.1002/hipo.22095.

39. Wilson, D.I., Watanabe, S., Milner, H., and Ainge, J.A. (2013). Lateral entorhinal cortex is necessary for associative but not nonassociative recognition memory. Hippocampus *23*, 1280–1290. https://doi.org/10.1002/hipo.22165.

40. Vandrey, B., Garden, D.L.F., Ambrozova, V., McClure, C., Nolan, M.F., and Ainge, J.A. (2020). Fan Cells in Layer 2 of the Lateral Entorhinal Cortex Are Critical for Episodic-like Memory. Curr. Biol. *30*, 169–175.e5. https://doi.org/10.1016/j.cub.2019.11.027.

41. Persson, B.M., Ambrozova, V., Duncan, S., Wood, E.R., O'Connor, A.R., and Ainge, J.A. (2022). Lateral entorhinal cortex lesions impair odor-context associative memory in male rats. J. Neurosci. Res. *100*, 1030–1046. https://doi.org/10.1002/jnr.25027.

42. Vivar, C., Potter, M.C., Choi, J., Lee, J.Y., Stringer, T.P., Callaway, E.M., Gage, F.H., Suh, H., and van Praag, H. (2012). Monosynaptic inputs to new neurons in the dentate gyrus. Nat. Commun. *3*, 1107. https://doi.org/10.1038/ncomms2101.

43. Woods, N.I., Vaaga, C.E., Chatzi, C., Adelson, J.D., Collie, M.F., Perederiy, J.V., Tovar, K.R., and Westbrook, G.L. (2018). Preferential Targeting of Lateral Entorhinal Inputs onto Newly Integrated Granule Cells. J. Neurosci. *38*, 5843–5853. https://doi.org/10.1523/JNEUROSCI.1737-17.2018.

44. Bilkey, D.K., Cheyne, K.R., Eckert, M.J., Lu, X., Chowdhury, S., Worley, P.F., Crandall, J.E., and Abraham, W.C. (2017). Exposure to complex environments results in more sparse representations of space in the hippocampus. Hippocampus *27*, 1178–1191. https://doi.org/10.1002/hipo.22762.

45. Kempermann, G., Kuhn, H.G., and Gage, F.H. (1997). More hippocampal neurons in adult mice living in an enriched environment. Nature *386*, 493–495. https://doi.org/10.1038/386493a0.

46. Colgin, L.L., Leutgeb, S., Jezek, K., Leutgeb, J.K., Moser, E.I., McNaughton, B.L., and Moser, M.B. (2010). Attractor-map versus autoassociation based attractor dynamics in the hippocampal network. J. Neurophysiol. *104*, 35–50. https://doi.org/10.1152/jn.00202.2010.

47. Lu, L., Leutgeb, J.K., Tsao, A., Henriksen, E.J., Leutgeb, S., Barnes, C.A., Witter, M.P., Moser, M.B., and Moser, E.I. (2013). Impaired hippocampal rate coding after lesions of the lateral entorhinal cortex. Nat. Neurosci. *16*, 1085–1093. https://doi.org/10.1038/nn.3462.

48. Leutgeb, J.K., Leutgeb, S., Treves, A., Meyer, R., Barnes, C.A., McNaughton, B.L., Moser, M.B., and Moser, E.I. (2005). Progressive transformation of hippocampal neuronal representations in "morphed" environments. Neuron *48*, 345–358. https://doi.org/10.1016/j.neuron.2005.09.007.

49. Kubie, J.L., and Muller, R.U. (1991). Multiple representations in the hippocampus. Hippocampus *1*, 240–242. https://doi.org/10.1002/hipo.450010305.

50. Witter, M.P. (2007). Intrinsic and extrinsic wiring of CA3: indications for connectional heterogeneity. Learn. Mem. *14*, 705–713. https://doi.org/10.1101/lm.725207.

51. Berdugo-Vega, G., Lee, C.C., Garthe, A., Kempermann, G., and Calegari, F. (2021). Adult-born neurons promote cognitive flexibility by improving memory precision and indexing. Hippocampus *31*, 1068–1079. https://doi.org/10.1002/hipo.23373.

52. Lee, H., Wang, Z., Tillekeratne, A., Lukish, N., Puliyadi, V., Zeger, S., Gallagher, M., and Knierim, J.J. (2022). Loss of functional heterogeneity along the CA3 transverse axis in aging. Curr. Biol. *32*, 2681–2693.e4. https://doi.org/10.1016/j.cub.2022.04.077.

53. Frechou, M.A., Martin, S.S., McDermott, K.D., Gökhan, Ş., Tomé, W.A., Coen-Cagli, R., and Gonçalves, J.T. (2022). Adult neurogenesis improves spatial information encoding in the mouse hippocampus. Preprint at bioRxiv. https://doi.org/10.1101/2022.11.30.518622.

54. Schmitzer-Torbert, N., Jackson, J., Henze, D., Harris, K., and Redish, A.D. (2005). Quantitative measures of cluster quality for use in extracellular recordings. Neuroscience *131*, 1–11. https://doi.org/10.1016/j.neuroscience.2004.09.066.

55. Skaggs, W.E., and McNaughton, B.L. (1998). Spatial firing properties of hippocampal CA1 populations in an environment containing two visually identical regions. J. Neurosci. *18*, 8455–8466. https://doi.org/10.1523/JNEUROSCI.18-20-08455.1998.

56. Jung, M.W., Wiener, S.I., and McNaughton, B.L. (1994). Comparison of spatial firing characteristics of units in dorsal and ventral hippocampus of the rat. J. Neurosci. *14*, 7347–7356. https://doi.org/10.1523/JNEUROSCI.14-12-07347.1994.

57. Muller, R.U., and Kubie, J.L. (1989). The firing of hippocampal place cells predicts the future position of freely moving rats. J. Neurosci. *9*, 4101–4110. https://doi.org/10.1523/JNEUROSCI.09-12-04101.1989.

Please cite this article in press as: Ventura et al., Increased flexibility of CA3 memory representations following environmental enrichment, Current Biology (2024), https://doi.org/10.1016/j.cub.2024.03.054

STAR★METHODS

KEY RESOURCES TABLE

REAGENT or RESOURCE	SOURCE	IDENTIFIER
Antibodies		
Rabbit anti-doublecortin	ABCAM	Cat #ab18723; RRID: AB_732011
Rabbit anti-Fos	Cell Signalling Technology	Cat #9F6; RRID: AB_2247211
Biotinylated IgG solution	Vectastain	Cat #PK-6100; RRID: AB_2336819
Avidin-biotin complex	Vectastain	Cat #PK-6100; RRID: AB_2336819
Chemicals, peptides, and recombinant proteins		
3,3-diaminobenzidine tetrahydrochloride	Sigma	Cat #D5637-1G
Cresyl violet	Sigma	Cat #C5042
Deposited data		
Datasets	This paper	https://doi.org/10.17630/afc19f9e-d927-4f15-a1d1-fbe17d84b989
Experimental models: Organisms/strains		
Rat: Lister Hooded	Envigo	Strain: HsdOla:LH
Software and algorithms		
TINT Spike sorting software	Axona	http://www.axona.com
MATLAB	Mathworks	https://www.mathworks.com/products/matlab
ZenPro	Zeiss	https://www.zeiss.com/microscopy/int/products/microscope-software/zen.html
NIS Elements	Nikon	https://www.microscope.healthcare.nikon.com/en_EU/products/software/nis-elements
ImageJ	Fiji	https://fiji.sc/
IBM SPSS Statistics	IBM	https://www.ibm.com
Other		
Axona Delrin Drive	Axona	http://www.axona.com
Axona Digital Acquisition System	Axona	http://www.axona.com
Gold Plating Solution	Neuralynx	https://neuralynx.fh-co.com
12.5 um Tungsten Wire	Axona	http://www.axona.com
Dual Lock Fastener	3M	SJ3560

RESOURCE AVAILABILITY

Lead contact

Further information and requests for resources and reagents should be directed to and will be fulfilled by the lead contact, James Ainge (jaa7@st-andrews.ac.uk)

Materials availability

This study did not generate new unique reagents.

Data and code availability

All data have been deposited on the University of ST Andrews PURE website and are publicly available as of the date of publication. DOIs are listed in the key resources table.

This paper does not report original code.

Any additional information required to reanalyze the data reported in this paper is available from the lead contact upon request.

Please cite this article in press as: Ventura et al., Increased flexibility of CA3 memory representations following environmental enrichment, Current Biology (2024), https://doi.org/10.1016/j.cub.2024.03.054

EXPERIMENTAL MODEL AND SUBJECT DETAILS

Animals

34 male Lister Hooded rats (Envigo, UK; average weight: 100-125g) were used in these experiments. 24 rats (EE: 12, ST:12) were used in the behavioural and Fos experiments, 10 (EE: 5, ST:5) were used in the recording experiment. All animals were housed in diurnal light conditions (12h light/dark cycle) with *ad libitum* access to water. Testing occurred in the light phase, 6-7 days a week. To encourage exploration during the tasks, the rats were food restricted to no less than 90% of their free feeding weight (15-25g per day). All experiments and surgeries were conducted under project licenses acquired from the UK home office and in accordance with national (Animal [Scientific Procedures] Act, 1986) and international (European Communities Council Directive of 22 September 2010 (2010/63/EU) legislation governing the maintenance of laboratory animals and their use in scientific research.

METHOD DETAILS

Housing conditions

Animals in the EE group were housed in groups of 4 (behavioural and Fos experiments) or 3 (recording experiment) in an enriched environment consisting of 3 standard cages connected with tunnels. The enriched environment was equipped with one disc running wheel, two polycarbonate houses, two hanging tubes, wooden ladders, and swings (Top, Figure S1A). These were maintained in the cage but moved around weekly. A new assortment of objects was introduced in the environment weekly, and sunflower seeds, banana chips and monkey peanuts were scattered in the environment twice a week to promote exploration. Animals in the standard group were housed in groups of 3 in standard laboratory cages (Bottom, Figure S1A). Each cage was equipped with a polycarbonate house, a hanging tunnel and nesting materials. For the recording experiment, following tetrode implant surgery, all animals were housed individually in high-top cages. However, to maintain enrichment exposure in the EE group, the EE rats were placed into an enriched environment (play pen) with their cage mates for 1 to 3 hours a day 6 to 7 days a week for the duration of the experiment. To habituate the animals to the play pen, daily exposure to the play pen started one month prior to surgery. The play pen was a squared environment with black wooden walls (wall length: 1 meter) equipped with toys of different materials and dimensions, a climbing wall, several wooden and plastic houses as well as cardboard mazes (Figure S2A). The play pen was in a separate room from the room where place cell recording took place, and exposure to the play pen always occurred after the recording for that day had finished

Behavioural experiment & Fos experiment

Apparatus

To manipulate the extent of memory interference in the tasks, the rats were tested on two versions of the Object-Context (OC) and of the Object-Place-Context (OPC) recognition memory tasks (similar and dissimilar conditions). In the similar condition, the test environment was a "morph box" made up of 32 rectangular pieces of white cable trunking (Electrical Supplies, TLC, UK; 7.5cm wide, 50cm high) that were held together in the inner surface with brown tape and masking tape. The morph box could be shaped as a square (each side: 62 cm) or as a circle (diameter: 79 cm) (Top, Figure S1B). The square was obtained by imposing a 90-degree bent in the wall every 8th rectangular piece, thus resulting in four walls made up of eight pieces in a straight line. The circle was obtained by joining together two rectangular pieces at a time, which were then arranged as to obtain a 16-sided polygon. The square and the circle had the same smooth black wooden floor. In the dissimilar condition, the test environment was a rectangular wooden box (32cm x 25.5cm x 22cm) that could be configured as Context A (smooth black walls and a black and white wire mesh floor) or Context B (wooden walls and a smooth floor with a red, a green, a yellow and a blue quadrant) (Bottom, Figure S1B). The floor and the walls of the environment were cleaned thoroughly between trials with Safe4 disinfectant (Safe Solutions, Ltd.) to remove odour cues. The environment was lit by two lamps, positioned at equal distances from the box.

Objects

The objects used in the tasks were household objects of different shapes, colours and material. These were roughly the size of the rat. The objects used during habituation were not reused during testing. During habituation and testing, one object was placed in the upper right quadrant of the box, and one in the upper left quadrant of the box. The objects were secured in place with white fastening tape (Dual Lock, 3M). Objects were cleaned with Safe4 disinfectant (Safe Solutions, Ltd.) before each trial. New sets of objects were used every day, and copies of each object were used for different trials to cover any odours. The objects used for the *c-Fos* experiment were identical copies of a white and blue ceramic mug, roughly the size of the rat.

Habituation

The rats were handled for 10 minutes per day during the week prior to testing. Habituation was repeated twice, once before testing in the similar version of the OC task, once before testing in the dissimilar version of the OC task. Before the similar version of the OC task, the contexts used during habituation were the square and circle versions of the morph box. Before the dissimilar version of the OC task, the contexts used during habituation were the dissimilar contexts A and B. On Day 1, the rats explored each context for 10 minutes in their cage groups. On Day 2, the rats explored each context for 5 minutes on their own. On Day 3, the rats explored each context for 5 minutes on their own. However, this time two random objects were placed in the upper quadrants (left and right) of the box.

Experimental timeline

Testing occurred in two phases: the Behavioural Experiment and the *c-Fos* Experiment. The Behavioural Experiment started four months after the rats had been placed in their housing condition. The *c-Fos* Experiment occurred roughly one month following the end of the Behavioural Experiment.

Behavioural experiment

The Behavioural Experiment occurred in 4 stages: similar OC task, dissimilar OC task, similar OPC task, dissimilar OPC task. Each task consisted of two sample phases and one test phase. Each phase lasted three minutes. In-between phases, the rat was placed in a holding cage for roughly one minute as the objects and contexts were cleaned, and the next testing phase was prepared.

A. OC tasks: In the first sample phase, the rat explored two identical copies of a novel object within one context. In the second sample phase, the rat explored two identical copies of a different novel object within the other context. The test phase occurred in one of the two contexts, and the rat explored one copy of the object that was explored in the first sample phase, and one copy of the object that was explored in the second sample phase. Thus, at test one object was in a context in which it had been experienced before (familiar OC configuration) and one object was in a context in which it had not been experienced before (novel OC configuration).

B. OPC task: In the first sample phase, the rat explored two different novel objects within one context. In the second sample phase, the rat explored copies of the same two objects in the opposite context. However, in the second sample phase each object was in the opposite quadrant compared to where it was in the first sample phase. At test, the rat was presented with two identical copies of one of the objects explored during the sample phases within one context. Thus, at test one object was in a context and in a location in which it had been experienced before (familiar OPC configuration), and one was not (novel OPC configuration).

For all tasks, in the similar condition, the contexts used were the square and the circle versions of the morph box. In the dissimilar condition, the contexts used were the dissimilar contexts described above. The OC and OPC stages lasted 4 days each. Each rat received one testing trial per day. For all tasks, the object that was novel at test, the quadrant and the context in which the object in the novel representation was presented, and the order in which the contexts were presented were counterbalanced across rats.

c-Fos *experiment*

The *c-Fos* Experiment occurred one month after the last day of the OPC dissimilar task and lasted three days. The rats were randomly assigned to either the Familiar or the Novel Condition.

A. Familiar Condition (EE n=5, ST n= 6): Over two days, the rats explored two copies of the same novel object within one of the similar, familiar contexts (circle or square) for 5 minutes each day. On the third day, the rat explored two copies of the same object explored in the prior two days in the same context (familiar object-context association) for 5 minutes.

B. Novel Condition (EE n=6, ST n= 6): Over two days, the rats were presented with two copies of the same novel object within one of the similar, familiar contexts (circle or square) for 5 minutes each day. On the third day, the rat explored two copies of the same object explored in the prior two days, this time in the other similar context (novel object-context association) for 5 minutes.

The context that was novel or familiar on the third day was counterbalanced across rats.

Behavioural data analysis

The behavioural videos were scored offline by the experimenter. A random sample of 25% of all test videos were scored by an independent scorer blind to condition to check for inter-rate reliability. Reliability between scorers was good with an intraclass correlation of 0.876 (2-way mixed model). The amount of time spent by the rat exploring each object was measured for all sample and test phases. Exploration was defined as moments when the animal's nose was roughly 2 cm within the object and directed towards it. For all test phases, a discrimination ratio was computed to determine whether the rat spent more time exploring the object in the novel configuration, using the following formula:

$$\text{Discrimination ratio} = \frac{(\textit{Time exploring object in novel configuration } (s) - \textit{Time exploring object in familiar configuration } (s))}{\textit{Total object exploration time } (s)}$$

For each animal, average discrimination ratios across the four days of testing were calculated for each task. Average means and standard errors of the mean were then calculated for each group. A positive discrimination ratio indicates that the rat spends more time exploring the object in the novel configuration, signalling memory for the previously encountered object-context (or object-place-context) configuration. Trials were total exploration during sample or test phase was less than 5s were excluded from the analysis. If more than 50% of the trials for a task met exclusion criteria for a rat, data for that rat was excluded from the analysis. This led to the exclusion of 1 ST rat from the Similar and Dissimilar OC and OPC tasks.

To examine general movement behaviour videos were scored using ANY-maze (Stoelting Europe). Three measures were taken. Average running speed across the session was calculated. A zone which comprised the area within 10cm of the wall was defined and average % of time spent in this region relative to the middle of the box was used to calculate thigmotaxis. Rearing was scored manually through the ANY-maze software.

Histology & DCX quantification

90 minutes following the completion of the test trial of the *c-Fos* Experiment, the animals were given a lethal dose of sodium pentobarbitol and transcranially perfused with phosphate-buffered saline (PBS), followed by roughly 350 ml of 4% paraformaldehyde (PFA). Brains were then extracted and stored in 20% sucrose overnight at 4 degrees. The brains were cut horizontally at 50um on a freezing microtome. For doublecortin (DCX) and *c-Fos* immunohistochemistry, 1 in 8 series were blocked for 2 hours in 20% Normal Goat Serum (NGS) prepared in 0.1% PBS-T (Triton). To stain against DCX, the slices were incubated in a primary antibody solution

prepared in 1% NGS in 0.1% PBS-T for 24h at room temperature on a stirrer. The primary antibody was rabbit anti-doublecortin (ABCAM, ab18723, 1:1000). To stain against *c-Fos*, the primary antibody solution contained rabbit anti-Fos (Cell Signalling Technology, 9F6, 1:1000). Slices were washed in PBS 5 times for 2 minutes before being incubated in biotinylated IgG solution (Vectastain Elite ABC Kit, 1:200) for 1h. Slices were the washed in PBS 5 times for 2 minutes before being immersed in avidin-biotin complex (Vectastain Elite ABC Kit, 1:50) for 1h. Sections were then reacted with nickel enhanced 3,3-diaminobenzidine tetrahydrochloride (Sigma) and mounted and cover slipped with DPX. DCX positive cells were imaged using a brightfield microscope (Zeiss ApoTome, 40x). DCX+ cells were quantified throughout the dorsal dentate gyrus (Bregma -3.68mm; Bregma -5.10mm) by an experimenter blind to experimental condition. Cells located in the granule cell layer and the subgranular zone, and whose cell body was clearly visible, were included in the count. For each image, the length of the dentate gyrus was measured in micrometres in ImageJ, and the DCX+ cell density was calculated for each image by dividing the number of DCX+ cells by the length of the dentate gyrus. Average DCX density counts across four dorsal sections were computed for each rat and used in the analysis

c-Fos *regions of interest (ROIs)*

Regions were identified with reference to the Paxinos & Watson (1991). Counts were taken from 6 subregions of the dorsal hippocampus (Bregma – 3.68, Bregma – 5.10) (suprapyramidal DG, infrapyramidal DG, proximal CA3, distal CA3, proximal CA1, distal CA1).

c-Fos *quantification*

Photographs of the regions of interest were taken using a 10x magnification (Zeiss ApoTome). Photographs of at least four, and a maximum of six, sections were taken for each region. Images were processed using ImageJ. To identify *c-Fos* positive cells, ImageJ took a mean grey scale value for each picture. *c-Fos* positive cells were included in the count if their brightness was more than 3 standard deviations greater than the mean grey scale for that picture. Density *c-Fos* counts were obtained by dividing the number of *c-Fos* positive cells by the size of the region they were counted from (in mm^2). To compare across regions with different cell densities, normalized cell density counts were computed by dividing raw cell density counts from each area by the mean count for that area across groups and conditions and multiplying the resulting number by 100.

Recording experiment

Surgical implantation of electrodes

Delrin Microdrives (Axona, LtD., UK) contained 8 tetrodes that could be moved independently in bundles of 2. Each tetrode was made of 12.5 micrometre tungsten wire (California Fine Wire, Grover City, CA). Tetrodes were placed in bundles of 2 in 33-gauge x 11 m steel cannulae. Each cannula was glued with superglue (3M, UK) to a plastic shuttle, and each microdrive had 4 plastic shuttles in total. Each shuttle was connected to a screw mechanism. The cannulae were organized in two rows, with 0.4 mm between rows. The cannulae were spaced roughly 0.6mm apart to allow us to target CA3 across the proximodistal axis. This resulted in roughly 1.8 mm between the most far right and the most far left cannulae in the drive. Before implantation, the tetrodes were cut to roughly 5 mm and plated with gold until the impedance of each electrode tip was between 100-200 kW. On the day of surgery, the rats were anaesthetised with Isoflurane in an induction chamber and injected with analgesic Metacam subcutaneously prior to being placed in a stereotaxic frame. The skull was then exposed and the microdrive was implanted in the left hemisphere and targeted at CA3 (3.72-4.0 posterior to Bregma), with the most proximal tetrodes implanted roughly 2.3 mm lateral to midline and the most distal tetrodes implanted roughly 4.1 mm lateral to midline. After the craniotomy, dura was cut, and the tetrodes were lowered 2.8 mm below dura. The implant was the secured to the skull using jewellers' screws and dental cement. A jeweller screw located near the front of the rat's skull was connected to the microdrive's ground wire.

Recording

Screening for place cells began one day after surgery. The microdrive was connected to a cable which provided unfiltered electrical signal from single electrodes to the recording system (DaqUSB, Axona Ltd., UK). Within the recording system, the signal was bandpass filtered (600-6000 Hz) and amplified 5000-20000 times with a unity-gain operational amplifier. An oscilloscope on a computer screen connected to the recording system allowed us to visualize filtered signals for each electrode (or channel) of each tetrode. During screening sessions, each channel in the oscilloscope was examined for spiking events. Additionally, population-based EEG signal was examined and sampled at 250Hz. Theta frequency, which is in the range of 8-12 Hz and is characteristic of the hippocampus, was looked for. Light-emitting diodes (LEDs) located on the head stage were used to detect the animal's location. If a unit was detected, a reference channel where no putative cells were present was used as a reference for the other channels. This was done for each tetrode. Additionally, the gain and the threshold for spiking event detection were adjusted to minimize noise and maximize signal for each tetrode. At the end of a recording session, tetrodes from which putative place cells were recorded were nudged down by roughly 10 micrometres. If no units were detected, the tetrodes were moved down by roughly 60 micrometres.

Behavioural apparatus

All recordings occurred in an electrophysiology suite consisting of a towel-line flowerpot (screening location) and a recording location. The recording location consisted of a black-curtained arena. The test box was placed on a black wooden floor positioned on a table in the centre of the arena. A white cue card positioned outside of the testing box and a switched off lamp located within the black-curtained arena functioned as global cues for the environment. The test box consisted of the "morph box" described above. For this experiment, the box was painted matte black to avoid the LEDs on the recording head stage reflecting on the walls, which would have resulted in inaccurate detection of the animal's location within the box. The morph box could be configured as a square with 62-cm sides, a circle with a 79-cm diameter, or four intermediate polygonal shapes (1:7, 2:6, 3:5, 4:4).[22] Critically, the centre of each testing environment was always in the same location across the distinct shapes.

Testing procedure

In the days prior to surgery, the rats were given 2 10-minute exposures to the square and the circle versions of the morph box for three days. On day 1, the rats explored the environments with their cage mates. On days 2-3, each rat explored the environments on his own. This was done to habituate the rats to the square and circle shapes, and to foraging for pieces of chocolate wheetos randomly thrown in the environment. When putative pyramidal cells were detected in at least one tetrode, testing and recording began. The testing procedure always began with a 10-to-15-minute exploration of either the square or the circle. Each exploration lasted 10-to-15 minutes and consisted in the rat foraging for pieces of chocolate wheetos randomly thrown in the box. The rat was always placed in the box facing the south wall. The recording session consisted of the initial square or circle exploration followed by exploration of the four intermediate shapes in sequential order, exploration of the circle (if the sequence started with the square) or the square (if the sequence started with the circle) and a repetition of the initial shape (full sequence, Top, Figures 4A and, S2B). This sequence was counterbalanced across days, as some days the rat experienced the shapes starting with the square, some starting with the circle. In-between exploration of distinct shapes, the rat was placed on the towel-line flowerpot (screening location) for roughly 5 minutes as the environment was morphed and the box was cleaned with Safe4 disinfectant. Data for the full sequence were collected from 3 standard-housed rats and 4 enriched rats. For some of the rats (2 standard-housed and 4 enriched rats), and on some days for the other rats, the session only included some, but not all, of the intermediate shapes (incomplete sequence, Bottom, Figure 4A). Data were included for a rat if the rat explored the first shape, the repetition of the first shape, and at least 2 shapes in-between.

Histology

Animals were first anaesthetised with Isoflurane in an induction chamber and placed in the stereotaxic frame. 9V current was then passed through each tetrode to create electrolytic lesions at the tetrode tips, to allow clearer visualization of the tetrode tracks. The animals were then given a lethal dose of sodium pentobarbitol and transcranially perfused with phosphate-buffered saline (PBS), followed by roughly 350 ml of 4% paraformaldehyde (PFA). The brain was then stored within the skull at 4 degrees overnight, until the brain was removed from the skull and stored in 20% sucrose in PBS at 4 degrees for 24h. The brain was then cut coronally on a freezing microtome at 50 micrometres and all sections including the hippocampus were mounted on slides and fixed overnight in a PFA bath. To visualize cell bodies, the brain sections were then stained with cresyl violet, and cover slipped with DPX. The cresyl violet protocol consisted of the slides being submerged in Xylene for 2 minutes, followed by sequential submersion in 100% alcohol and 50% alcohol for 1 minute in each solution. The slides were then washed with tap water for 1 minute and placed in Cresyl Violet for 2 minutes. Prior to being cover slipped with DPX, the slides were then submerged again in water, and in the 50% and 100% alcohol solutions for roughly 1 minute.

Tetrode location along the CA3 transverse axis

For each animal the distance between the location of the tetrode tip and the most proximal point of CA3 was measured using ImageJ.[52] This value was then divided by the total length of CA3. This resulted in a value ranging from 0 (most proximal CA3) and 1 (most distal CA3).

Place cell identification

TINT (Axona) was used to sort the raw recording data. Spike clusters were first generated using KlustaKwik, which automatically sorts raw spike data into clusters based on principal components (PCs) such as amplitude and energy. The resulting clusters were then either deleted (if they did not look like neuronal spikes) or manually refined to reduce noise. Putative pyramidal cells were distinguished from putative interneurons based on spike width. The recording arena was divided into 5 cm x 5 cm bins. Place fields were constructed by summing the total number of spikes that occurred in each location bin (5x5cm), divided by the time that the rat spent in that location. Place fields were defined as contiguous region of ^{3} 9 (5cm x 5cm) bins where the minimum firing rate was ^{3} 0.2 Hz and ^{3} 20% of the peak firing rate for that cell in that shape. Additionally, for each place field a smoothing value of 5 cm SD Gaussian centred on each bin was applied. Finally, a shuffling procedure was used to define place cells; for all putative place cells, the times at which they fired were shuffled relative to the locations at which they fired. This yielded a randomized distribution of spatial information scores. By doing so, 1,000 randomized rate maps, and spatial information scores, were created for each putative place cell. Any cell with a spatial information score that was above the 99^{th} percentile of this randomized distribution of information scores was considered a place cell.[40] Units with at least one place field in at least one shape within the session in which they were recorded were included in the global remapping analysis. For the rate remapping analysis, units with at least one place field in each shape within the session in which they were recorded were included.

Quantification of cluster quality

The quality of each cluster was calculated as previously described[54] using a MATLAB script which measured a squared Mahalanobis distance for each cluster. In particular, for each cluster *c* with *n* spikes, the squared Mahalanobis distance is calculated as:

$$D^2_{i,C} = (X_i - \mu_c)^T \sum_c^{-1} (X_i - \mu_c)$$

where X_i= any vector with features for spike *I*, and μ_c = the main vector with features for cluster *c*. Thus, a squared Mahalanobis distance is the distance between the nth closest spikes that do not belonging to cluster *c* and the centre of cluster *c*. High values point to better cluster quality and better isolation. Units with an isolation distance of > 20 were classified as highly isolated, units with an isolation distance between 10 and 20 were classified as intermediately isolated and units with an isolation distance < 10 were classified as poorly isolated. Units were included in the analysis if they were intermediately or highly isolated in at least one shape within the session. The automatic isolation distance calculation could only be performed on clusters with a good connection on all four channels per each tetrode. If a channel was grounded or did not have a good connection, isolation distance for that cluster was assessed by comparing those clusters to clusters for which automatic isolation distance could be calculated.

Analysis of place cell characteristics

The MATLAB script computed firing maps for each cell, which depict the firing rate for a cell in each bin using a colour ranging from blue (lowest firing rate, cell not active) to red (maximum firing rate, cell maximally active). The firing rate map was analysed for the whole 10-to-15-minute recording trial in each shape, and the following place cell properties were computed: spatial information content, selectivity, spatial coherence, average firing rate in the field, peak firing rate in the field, and place field size. To look at the effect of group on place cell properties, these place cell properties were analysed for all cells that had a place field in the square shape and place cell characteristics in the square were compared for each existing session across groups. The square was picked as a representative shape that could be used to compare the two groups. The spatial information score indicates the amount of information that one can get about the location of the animal based on each spike of the cell. This is calculated as[55]:

$$\text{Spatial Information} = \sum P_i \frac{\lambda_i}{\lambda} log_2 \frac{\lambda_i}{\lambda}$$

The spatial information score is measured in bits/spike, and it indicates the time that the rat spends in a given bin *i*/total recording time. In the equation, λ_i = average firing rate in a unit in the *i*-th bin, λ = overall firing rate, and P_i = the probability of finding the rat in the *i* bin. The average in-field firing is calculated by dividing the total number of spikes within the place field by the time the time the rat spent in that location, and the peak in-field firing rate is the maximum firing rate of the cell in its place field (in Hertz (Hz)). Sparsity indicates how specific the place field of a cell is compared to the total area of the test environment. This is calculated as[56]:

$$\text{Sparsity} = \frac{(\lambda)^2}{(\lambda^2)} = \frac{\left(\sum p_1 \lambda_1\right)^2}{\left(\sum p_1 {\lambda_1}^2\right)}$$

where λ_i = the average firing rate of a unit in the *i*-th bin, λ = the overall firing rate, and P_i = the probability of finding he rat in the *i* bin. Selectivity indicates how specific the spikes of a cell are to the place field of the cell, and it is calculated as:

$$\text{Selectivity} = \frac{\textit{maximum firing rate}}{\textit{average firing rate}}$$

Spatial coherence, instead, is used to determine to what extent firing rates within a pixel are matched with firing rates in adjacent pixels,[57] and it is an indication of how coherent a firing field is. This is calculated as the z-transformed correlation between firing rates in each pixel and the firing rates in eight adjacent pixels of the environment.

Finally, if the same unit was recorded over more than one day, the recording in which the cell had the highest spatial information score was included in the analysis.

Analysis of global remapping and subset switching

Place cells that had a field in at least one shape within the session in which they were recorded were included in the main global remapping analysis. This was done using a MATLAB script by correlating rate maps of a cell across the initial shape (either square or circle) and each of the subsequent shapes in the session. Each pixel of the rate map from the first shape in the session was correlated with each pixel of the rate map of the same cell in each of the subsequent shapes within the same session. This generated a Pearson's correlation coefficient for each comparison (here referred as trial). Correlation values ranged between -1 and -1, where correlations of 1 indicate identical maps and 0 indicate no relationship between bin values in the 2 maps. Critically, bins that were not visited by the animal were discarded from the analysis. Cells that did not have a field in one or more of the shapes in the session (as defined in the place cell identification section), or whose fields were only present in one shape, were considered as subset switching, which is a specific form of global remapping. Finally, for each animal a global remapping value was computed. This was done by calculating, for each animal, the average spatial correlation value for all cells recorded from sessions including the full sequence. Averaged values from each animal were then used in the correlation with the tetrode location values.

Analysis of rate remapping

The rate remapping analysis was conducted on place fields, rather than on units. Place fields that were present in all shapes within the session in which they were recorded were included in the rate remapping analysis. Rate remapping was calculated across the first shape in the session and each subsequent shape as the normalized "rate difference" between two.[47] This was done by taking the absolute difference in firing rate for a field between two shapes and dividing it by the sum of the firing rates for that field across the same two shapes. Rate remapping values were calculated for both the average in-field firing rates and the peak in-field firing rates. A rate remapping value of 0 indicates that a cell's firing rate is identical across two trials, as rate remapping values increase this indicates a greater difference in firing rates between two trials. Greater values indicate greater rate remapping across the two shapes. Finally, for each animal an average rate remapping value was computed. This was done by calculating, for each animal, the average rate difference across the full sequence for all cells, and then averaging that number across all cells recorded for each animal. Only cells that were recorded from sessions including the full sequence were included in the analysis. Averaged values from each animal were then used in the correlation with the tetrode location values.

QUANTIFICATION AND STATISTICAL ANALYSIS

Statistical analyses were conducted using SPSS (IBM, version 28). Prior to analysis, normality of data was checked using the Shapiro-Wilk test. If the Mauchly's test was significant, Greenhouse-Geisser corrections were used. To compare rat performance across groups, univariate ANOVAs were run for each task on the discrimination ratios for each group (EE vs ST). To determine whether the average discrimination ratios were significantly greater than chance level, one-sample t-tests against the value of 0 were conducted on the discrimination ratios for each group for each task. To compare object exploration during the test phase across groups, univariate ANOVAs were run for each task on the total object exploration during test (s) for each group (EE vs ST). Additionally, a Mixed Effect ANOVA with Sample (1 vs 2), Task (OC and OPC) and Similarity (Similar vs Dissimilar) as within-subjects factors and Group (EE vs ST) as between-subjects factor was run on the total object exploration (s) to assess differences in the amount of time the rats spent exploring the objects during encoding. A univariate ANOVA was used to compare DCX density counts across the enriched and the standard groups. To determine whether there was a relationship between performance in the tasks and levels of adult hippocampal neurogenesis, Pearson's product-moment correlation coefficients were calculated with DCX density against discrimination ratios for each task for each animal. Normalized *c-Fos* density counts were analysed in the dorsal hippocampus (SPDG, IPDG, pCA3, dCA3, pCA1, dCA1). A Mixed Effect ANOVA with Group (Enriched, Standard) and Condition (Familiar, Novel) as between-subjects factors and ROIs as within-subjects factor was used to compare normalized *c-Fos* density counts across regions, groups and conditions.

To determine whether there was a significant difference across the enriched and standard groups in place cell properties, Kruskal-Wallis H-tests were conducted with Group (Enriched and Standard) as Fixed Factor. For the place cell properties, the values for the shape "square" were included in the analyses for each cell that had a place field in the square shape. This was done to assess group differences in place cell properties within a representative shape. For the rate remapping analysis, a Mixed Effect ANOVA was run with Session as within-subjects factor and Group as between-subjects factor on place cells recorded from session including all possible configurations of the morph box. A Generalized Linear Mixed Models (GLMM) were run with Cell as Random Factor and Group and Trial as Fixed Factors on rate differences from place fields that were recorded in sessions that included the initial shape (square or circle), a repetition of the first shape and at least two shapes in-between. This was done to include cells recorded from incomplete sessions. To be included in the rate remapping analysis, the place field had to be present in all shapes within the session. Following significant interactions, Bonferroni-corrected pairwise contrasts were performed to compare rate differences across trials and groups. For the main global remapping analysis, a GLMM was run with Cell as Random Factor and Group and Trial as Fixed Factors on spatial correlation values across the first shape and each subsequent shape. This analysis included all units with a field in at least one shape in the session. To determine whether a higher percentage of place cells showed subset switching across the enriched and the standard groups, observed frequencies of place cells showing subset switching were compared across experimental groups using a Chi Square test of independence. Finally, Pearson's correlations (or Spearman's correlation) were run between global remapping scores/rate remapping scores and tetrode location values (distance from the most proximal side of CA3) for each animal.